Polarization reduction in half-metallic Heusler alloys: the effect of point defects and interfaces with semiconductors

2007 J. Phys.: Condens. Matter 19 315215

(http://iopscience.iop.org/0953-8984/19/31/315215)

IOP PUBLISHING JOURNAL OF PHYSICS: CONDENSED MATTER

J. Phys.: Condens. Matter **19** (2007) 315215 (17pp) doi:10.1088/0953-8984/19/31/315215

Polarization reduction in half-metallic Heusler alloys: the effect of point defects and interfaces with semiconductors

Silvia Picozzi[1] **and Arthur J Freeman**[2]

[1] Consiglio Nazionale delle Ricerche—Istituto Nazionale di Fisica della Materia (CNR-INFM), CASTI Regional Laboratory, 67100 Coppito (L'Aquila), Italy
[2] Department of Physics and Astronomy and Materials Research Center, Northwestern University, Evanston, IL 60208, USA

E-mail: silvia.picozzi@aquila.infn.it

Received 2 November 2006
Published 3 July 2007
Online at stacks.iop.org/JPhysCM/19/315215

Abstract

Half-metallic full-Heusler alloys represent a promising class of materials for spintronic applications. However, (i) intrinsic point defects in Heusler compounds can be detrimental with respect to their predicted 100% spin polarization at the Fermi level and (ii) when joined to mainstream semiconductors the presence of interface states—which destroys half-metallicity—can degrade their performance. Here, we present an overview of recent first-principles calculations performed to explore both these issues. In particular, we focus on *ab initio* FLAPW calculations performed for Co_2MnGe and Co_2MnSi in the presence of intrinsic defects (such as stoichiometric atomic swaps as well as non-stoichiometric antisites) and when interfaced with GaAs and Ge. Our findings show that Mn antisites, due to their low formation energies, can easily occur, in excellent consistency with experimental observations, and that they do not destroy half-metallicity. On the other hand, Co antisites, which also show a modest formation energy, give rise to defect states at the Fermi level. As for the [001]-ordered interfaces, we show that the strong hybridization in proximity to the junction gives rise to rather broad interface states that locally destroy half-metallicity. However, the bulk gaps (both in the minority spin channel for the Heusler alloy and for both spin channels in the semiconducting side) are fully recovered within a few layers away from the junction.

(Some figures in this article are in colour only in the electronic version)

1. Introduction

Half-metallicity (i.e. the occurrence of a metallic and semiconducting density of states (DOS) in the majority and minority spin channels, respectively, of a ferromagnetic material) and the resulting 100% spin polarization at the Fermi level are peculiar properties, which open exciting routes towards promising spintronic devices. In particular, full-Heusler alloys such as Co_2MnX (X = Si, Ge, Sn), due to their high Curie ordering temperatures and their predicted half-metallicity, have been at the centre of many experimental and technological studies focused on their use in spintronic devices, such as magnetic tunnel junctions as well as spin injection into semiconductors. For example, Kämmerer *et al* [1] have integrated Co_2MnSi as one magnetic electrode into magnetic tunnel junctions (MTJs) with an AlO_x barrier and the resulting tunnel magnetoresistance-effect amplitude was determined as a function of temperature. Its spin polarization was estimated to be 61% at 10 K. Similarly, Sakuraba *et al* [2] focused on magnetic tunnel junctions with a stacking structure of epitaxial Co_2MnSi/AlO barrier/polycrystalline $Co_{75}Fe_{25}$. These MTJs exhibited magnetoresistance (MR) ratios of 70% at room temperature (RT) and 159% at 2 K, the highest values to date for MTJs using a Heusler alloy electrode. Moreover, Dong *et al* [3] demonstrated electrical spin injection from the Heusler alloy Co_2MnGe into a p–i–n $Al_{0.1}Ga_{0.9}As$/GaAs light emitting diode, with a maximum steady-state spin polarization of approximately 13% at 2 K measured in two types of heterostructures. The injected spin polarization at 2 K was calculated to be 27% based on a calibration of the spin detector using Hanle effect measurements. Although the dependence on electrical bias conditions was qualitatively similar to Fe-based analogously designed spin injection devices, it was found that the spin polarization injected from Co_2MnGe decayed more rapidly with increasing temperature.

Although some experimental results are certainly encouraging, the measured spin polarization, P, is often much lower than the full spin polarization predicted from first-principles calculations [4–6] based on density functional theory. In the past few years, several mechanisms have been suggested as possible causes of the reduction of P. For example, the temperature dependence of the magnetization and the spin polarization at the Fermi level in half-metallic ferromagnets (such as NiMnSb) was studied by Lezaic *et al* [7]. The thermal properties were studied by mapping *ab initio* results onto an extended Heisenberg model which includes longitudinal fluctuations and was solved by a Monte Carlo method. In [7] it was found that, due to the hybridization of states forming the half-metallic gap that depends on thermal spin fluctuations, the polarization can drop abruptly at temperatures much lower than the Curie point.

Moreover, it was also pointed out that the inclusion of correlation effects (which are often neglected within density functional theory) might change the value of the predicted spin polarization and can improve the agreement with experiments. For example, Kandpal *et al* [8] pointed out that, in the local density approximation (LDA), the minimum total energy of Co_2FeSi was found for the experimental lattice parameter, but the calculated magnetic moment was too low (about 12% underestimate). In addition, half-metallic ferromagnetism and a magnetic moment equal to the experimental value of 6 μ_B were predicted only after increasing the lattice parameter by more than 6%. To overcome the discrepancies with experiments, the LDA + U scheme was used to better treat on-site electron correlations. For Co_2FeSi, these calculations showed that an effective Coulomb exchange interaction $U_{\text{eff}} = U - J$ in the range of approximately 2–5 eV leads to half-metallic ferromagnetism and to the measured integer magnetic moment at the measured lattice parameter. Finally, it was shown that correlation may also lead to a loss of half-metallic behaviour if the correlation becomes too strong (above 2 eV for Co_2MnSi and above 5 eV for Co_2FeSi). These findings indicate that on-site correlation may play an important role in the description of Heusler compounds with localized moments.

Surface effects were also pointed out as mechanisms to reduce P. Ishida *et al* [9] performed pioneering simulations on the (001) and (111) Co_2MnGe and Co_2MnSi films. They showed that whether the film becomes half-metallic or not depends on its thickness and its surface; moreover, the (111) film with the Si or Ge atom surface was predicted to be half-metallic. Recently, the stability, as well as the electronic and magnetic structure, of Co_2MnSi (001) thin films for 15 different terminations were studied by Hashemifar *et al* [10] within density functional theory. The pure Mn termination, due to its strong surface–subsurface coupling, was found to preserve the half-metallicity of the system, while surface states appeared for the other terminations. Galanakis [11] focused on the electronic and magnetic properties of the (001) surfaces of several full- and half-Heusler alloys. The MnSb-terminated surfaces of the half-Heusler compounds (such as NiMnSb) showed properties similar to those of the bulk and, although full half-metallicity was lost, a high spin polarization at the Fermi level was obtained. In full-Heuslers, Co_2MnGe and Co_2MnSi surfaces were predicted to lose the half-metallic character, with a resulting spin polarization at the Fermi level close to zero.

In addition to the mechanism previously pointed out, there are two effects that might lead to a reduction of P, which will be the subject of the present review: the occurrence of (i) defect states in the bulk materials due to point defects (such as antisites, atomic swaps, etc) and (ii) interface states at the Heusler/semiconductor junctions. These two important topics will be studied for two well characterized full-Heusler alloys, namely Co_2MnGe and Co_2MnSi. Both these compounds show a very high T_C (of 985 and 905 K for Co_2MnSi and Co_2MnGe, respectively [12, 13]), along with the half-metallicity [4], predicted from first principles in the 1990s. In addition, their $L2_1$ cubic crystal structure well matches that of the mainstream zinc-blende semiconductors. Last but not least, the lattice mismatch is very small (the lattice constants of Co_2MnSi and Co_2MnGe are 10.68 au and 10.85 au, respectively, which are remarkably close to that of, say, GaAs, 10.683 au). All these characteristics lead Co_2MnSi and Co_2MnGe to be included in the list of most promising materials for spintronic applications.

In this review, we will focus on two aspects that might cloud their potentialities and which have therefore to be kept under control, i.e. (i) intrinsic point defects in Co_2MnGe and Co_2MnSi and (ii) two mainstream semiconductors (SCs), such as GaAs and Ge, interfaced with Co_2MnGe along the [001] growth axis.

2. Computational and structural details

Our calculations were performed within the density-functional theory using both the local spin density approximation (LSDA) [14] and the generalized gradient approximation (GGA) [15] for the exchange–correlation potential. In particular, in the case of interfaces, we performed LSDA calculations, motivated by the fact that experimental semiconductor lattice constants are generally closer to LSDA values, whereas GGA tends to overestimate them. On the other hand, GGA works better when a high percentage of magnetic ions is present in the unit cell. We therefore chose to perform GGA calculations in the case of defects. All the simulations were performed by means of the highly accurate all-electron full-potential linearized augmented plane wave (FLAPW) [16] method. Muffin tin radii were chosen to be $R_{MT} = 2.1$ au for all the atomic species; angular momenta (wavevector) up to $l_{max} = 8$ ($K_{max} = 3.6$ au) were used for the expansions of both wavefunctions and charge density. The Brillouin zone was sampled using special $\mathbf{k}$ points according to the Monkhorst–Pack scheme [17].

As for the purpose of calculating the electronic group velocity $v(\mathbf{k}) = (1/\hbar)\partial\varepsilon(\mathbf{k})/\partial\mathbf{k}$, the eigenenergies $\varepsilon(\mathbf{k})/\partial\mathbf{k}$ over a set of about 80 $\mathbf{k}$-points were used for a spline fitting of the bands over the Brillouin zone. The resulting interpolating Fourier series was then used to calculate the required energy derivative [18].

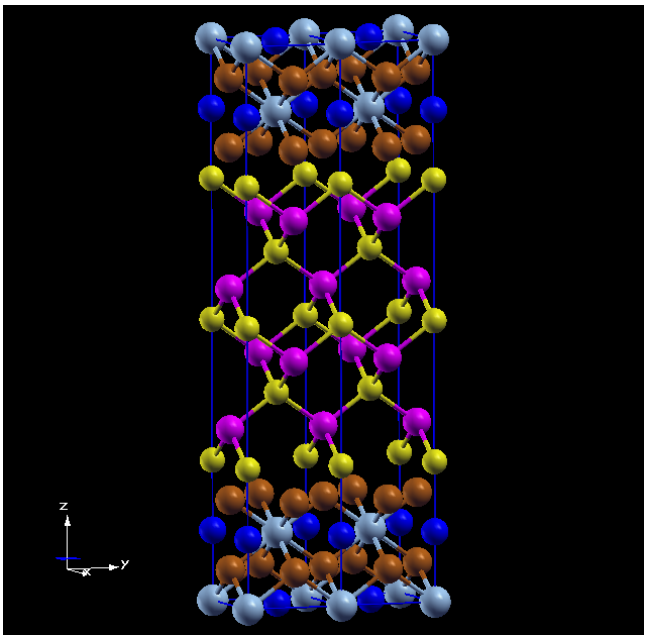

Figure 1. Sketch of the [001]-ordered $Co_2MnGe/GaAs$ interface, terminated by Co and As. For clarity, we show only a few atomic layers; in particular, this unit cell shows nine layers of GaAs and seven layers of Co_2MnGe, whereas 11 and 13 layers of GaAs and Co_2MnGe, respectively, were used in the simulations. Grey (light grey) and blue (black) spheres in the side layers shows the Mn and Ge atoms; the Co planes in the side layers are shown by orange (dark grey) spheres. In the semiconducting central part, yellow (small) and purple (large) spheres represent As and Ga atoms. The vertical axis shows the [001] growth direction.

In order to simulate the [001]-ordered Heusler/semiconductor interfaces, we considered supercells containing up to 13 Co_2MnGe + 11 semiconductor (SC) layers, with the Heusler compound tetragonally strained to match the semiconducting substrate; a representative example of the geometry used is shown in figure 1. In order to address the dependence of the results on the interface geometry, calculations were performed for all possible terminations (i.e. Mn–Ge/As, Co/As, Mn–Ge/Ga, Co/Ga in $Co_2MnGe/GaAs$).

As for calculations related to defects, we employed a 32-atom unit cell, obtained by considering the $L2_1$ bulk unit cell (with four atoms) and doubling its Bravais vectors (i.e. the defective cell is $2 \times 2 \times 2$ times the $L2_1$ unit cell). In order to check the convergence of the results as a function of the unit-cell dimensions, we performed some test calculations using 64 atoms; we obtained only small quantitative changes in the relevant properties, but, qualitatively, the physical results are the same as those obtained for the smaller 32-atom cell [19]. The lattice constant was kept fixed to the calculated bulk equilibrium value [5]—within the generalized gradient approximation (GGA) [15], i.e. $a(Co_2MnGe) = 10.84$ au and $a(Co_2MnSi) = 10.65$ au. Internal degrees of freedom were fully relaxed according to *ab initio* atomic forces.

The formation energy was evaluated as [20]

$$\Delta E = E^{\mathrm{def}} - E^{\mathrm{id}} + n_{\mathrm{Mn}}\mu^0_{\mathrm{Mn}} + n_{\mathrm{Co}}\mu^0_{\mathrm{Co}} + n_{\mathrm{X}}\mu^0_{\mathrm{X}} \tag{1}$$

where E^{def} and E^{id} are the total energies of the unit cell with and without defect, respectively; in forming the defect, the n_i take into account that n_i atoms are transferred to or from a chemical

Table 1. Formation energy (in eV) and total magnetic moments (in Bohr magnetons) for different defects in Co_2MnGe and Co_2MnSi hosts.

	Co_2MnSi		Co_2MnGe	
	ΔE	M_{tot}	ΔE	M_{tot}
Co antisite	0.80	38.01	0.84	38.37
Mn antisite	0.33	38.00	0.33	38.00
Co–Mn swap	1.13	36.00	1.17	36.00
Mn–Si swap	1.38	40.00	—	—

reservoir that has a characteristic energy μ_i^0. In our case, we chose as the stable phase for element i (i = Mn, Co, X (= Si, Ge)) the [001]-ordered fcc antiferromagnetic Mn [21], ferromagnetic hcp Co [21] and the Si (or Ge) diamond-like structure, respectively. Charged defects or competing crystalline phases that might be formed during defective growth are not taken into account.

Finally, the equilibrium concentration of the defect at temperature T, considering a Boltzmann-like distribution, can be estimated as [22]

$$D_{def} = N_{sites} \exp\left(-\frac{\Delta E}{k_B T}\right) \tag{2}$$

where N_{sites} is the number of available sites.

3. Intrinsic defects in full-Heusler alloys: results and discussion

3.1. Energetics

In table 1, we report the calculated formation energies for all the defects considered in the two different matrices; we also show the total magnetic moment in the unit cell (see the following paragraph for the related discussion). Recall that both Co_2MnGe and Co_2MnSi in their bulk phases show a total magnetic moment of 5 μ_B (or, equivalently, a magnetic moment of 40 μ_B in the 32-atom unit cell used for the defect calculations) [5].

We observe that the considerably small value obtained for the formation energy of the Mn antisite (ΔE = 0.33 eV) suggests that this kind of defect is likely to be formed during Co_2MnSi growth. In particular, considering a temperature T = 1523 K, suitable for a triarc Czochralski growth of bulk Co_2MnSi [23], the Mn antisite concentration can reach the high value of about 0.4×10^{22} cm^{-3}, corresponding to about 8%. This is in excellent agreement with the reported experimental value of 5–7% [23]. However, we point out that ours is quantitatively only a rough estimate, since equation (2) is strictly valid in the limit of very low concentrations, that are greatly exceeded when considering more than a few per cent.

For the Co antisite, a slightly higher formation energy is calculated. According to equation (2), this increase results in a concentration which is almost two orders of magnitude smaller than that obtained for the Mn antisite. Therefore, although their occurrence can certainly not be excluded, these defects are expected to have a relatively small density. This is actually at variance with experiments, which found Co and Mn antisites occurring with more or less the same concentrations. We need to point out, as previously noted, that some errors may arise from the quantitative estimate of the concentrations for a high defect density: equation (2) shows that small uncertainties in ΔE (due to the finite size of the unit cell, **k**-point sampling or other computational details) result in large errors in the defect concentration.

Let us now consider atomic interchanges such as Mn–Co swaps; this defect can also be viewed as the sum of two different Mn and Co atomic antisites that tend to cluster. This complex

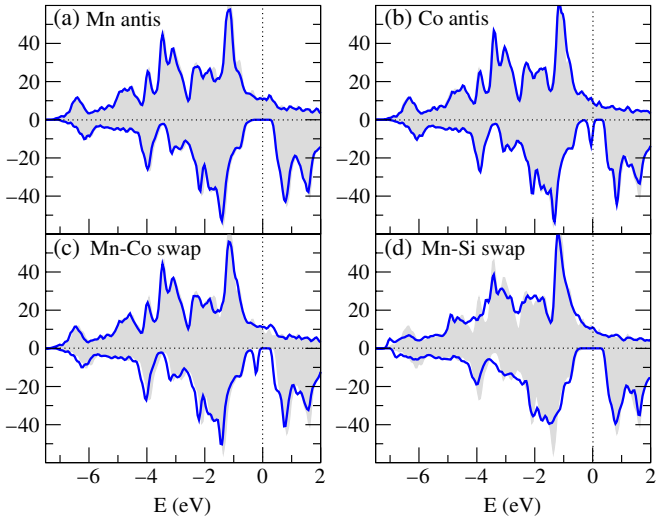

Figure 2. Total DOS for (a) Mn antisite, (b) Co antisite, (c) Mn–Co swap and (d) Mn–Si swap. The majority (minority) spin contribution is shown on the positive (negative) y-axis. The shaded grey area shows the ideal non-defective Co_2MnSi case, whereas the bold (blue) line shows the defective case. The zero of the x-axis shows the Fermi level.

defect shows a rather high formation energy; however, if we compare its formation energy with the sum of the separated defects (Mn antisite and Co antisite) we obtain a very similar value. This might indicate that point defects have more or less the same probability to cluster, leading to this kind of disorder, or to remain isolated.

Finally, we focus on the Mn–Si swap, which shows, however, the highest formation energy among the cases studied. Therefore, the occurrence of an appreciable concentration of this kind of defect is highly unlikely. This is consistent with experiments which show that the Si site is almost fully occupied by Si, indicating that any disorder in Co_2MnSi does not involve Si. On the other hand, our findings are at variance with other first-principles predictions for the NiMnSb half-Heusler alloy: according to Orgassa *et al* [24], the Mn–Sb (analogous to the Mn–Si here considered) disorder seems likely.

3.2. Electronic structure: density of states and magnetic moments

We now discuss the electronic and magnetic properties of the system, focusing in particular on the defect-induced changes of the half-metallicity. In figure 2, we present the total density of states (DOS) of both the defective and the ideal systems. Moreover, in figure 3 we show the defect induced modifications in the magnetic moments for the atoms surrounding the defect and compare them to the ideal case.

For the Mn antisite, the comparison in figure 2(a) shows that the defect induces only minor modifications—such as features at -1.5 and -0.8 eV for the majority spin states; on the other hand, due to the Mn antisite, a rigid shift of about 0.05 eV towards higher binding energies occurs in the minority spin channel. This results in a small increase of the spin-gap (0.34 and 0.39 eV in the ideal and defective systems, respectively). However, half-metallicity is preserved even in the presence of the Mn antisite, the total magnetic moment being 38 μ_B and 40 μ_B in the defective and ideal unit cells, respectively. Interestingly, the half-metallic character is kept thanks to a charge balance granted by the majority component only. In fact, in this case, the total charge differs from the ideal case by $\Delta Z = -2$ electrons; since the

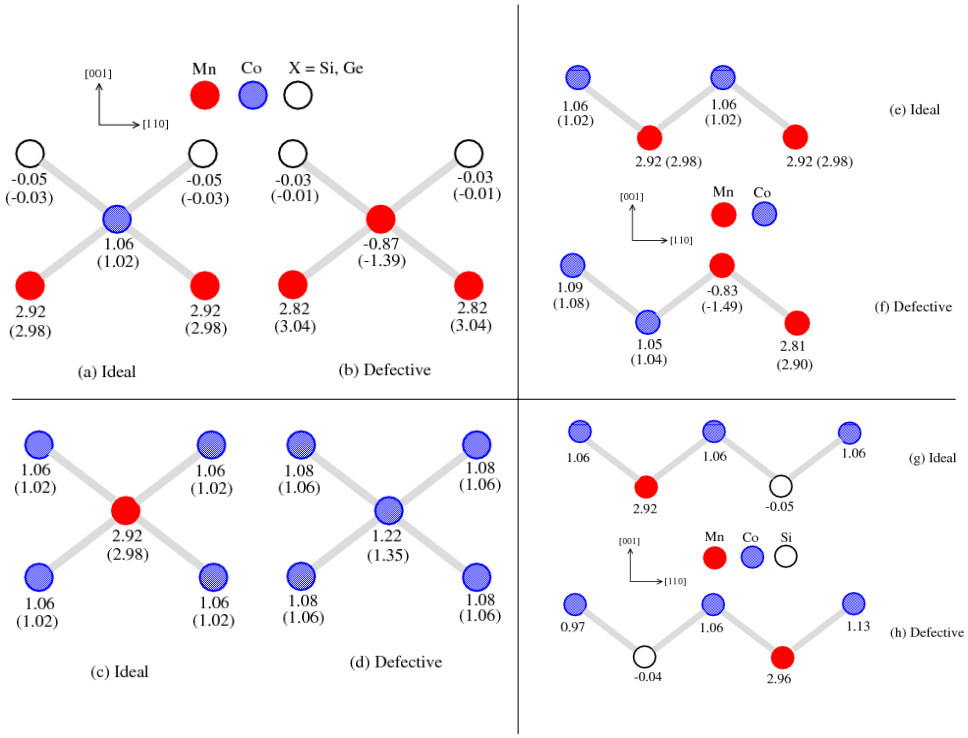

Figure 3. Effects of point defects on the muffin-tin magnetic moments in Co_2MnSi (values in parenthesis denote corresponding values for Co_2MnGe). Only the region around the defect is shown. Upper left panel: (a) ideal and (b) defective Mn-antisite cases. Lower left panel: (c) ideal and (d) defective Co-antisite cases. Upper right panel: (e) ideal and (f) defective Co–Mn swap. Lower right panel: (g) ideal and (h) defective Mn–Si swap.

number of occupied states in the minority spin channel does not change (see figure 2(a)), $\Delta N_- = 0$), then the variation of occupied states in the majority component must account for the total ΔZ (i.e. $\Delta N_+ = -2$ electrons). In particular, the two-electron states appear as a new peak at ∼0.3 eV above E_F, almost entirely due to the Mn-antisite d states, as shown by the corresponding feature in the DOS projected (PDOS) on to the Mn defective site (see the shaded area in figure 2(a)). Our results are particularly relevant in the spin-injection framework: even if the Mn antisite defects—due to their low formation energies—are most likely to occur during Co_2MnSi growth, the most important property of this Heusler alloy, i.e. its half-metallicity, is kept. Therefore, experimental results reporting a polarization lower than the expected 100% should be ascribed to surface effects [9] or other types of bulk defects (such as Co antisites [25, 26]—see below, vacancies, interstitials, etc). Further insights can be gained from the magnetic moments of the different atomic species. In figures 3(a) and (b), we report a schematic view of the region close to the defect (i.e. the Mn antisite and its first-nearest neighbours along the [110] direction) as compared with the same region in the ideal Heusler alloy, including the relative magnetic moments in the MT spheres. Here and in the following similar figures, we report only these few atoms since (i) other symmetry directions (i.e. $[1\bar{1}0]$) show an equivalent behaviour and (ii) farther atomic shells do not show variations of their magnetic moments larger than 1% with respect to their bulk values and/or are below our numerical precision (0.01 μ_B). The central Mn antisite accounts for all the defect-

induced reduction of 2 μ_B in the total magnetic moment, since it has a magnetic moment of -0.87 μ_B and substitutes for a Co having a magnetic moment of 1.06 μ_B. The large change in the atomic magnetization (which also reverses its sign) on the defect site shows that a large rearrangement of the charge and spin densities occurs when the defect is introduced, as shown by the completely different projected DOS (not reported) on the Mn defect site compared to Mn in bulk Co_2MnSi. Only small changes are observed on its nearest neighbours, which shows that the defect-induced effects are efficiently screened out in the Co_2MnSi matrix; incidentally, these findings support our computational choice of a relatively small unit cell.

For the Co antisite, an analysis of the total DOS (see figure 2(b)) shows a defect-induced dramatic change in the conducting character: half-metallicity is lost, due to a very sharp peak located just in proximity to E_F. As shown in figure 2(b), there is an almost exact superposition between the ideal and defective total DOS, except for the peak at E_F. The projected density of states (not shown) reveals that this is almost entirely due to the antisite Co d states. In particular, these states accommodate two electrons (see below) and are doubly degenerate at the Brillouin-zone centre with e_g symmetry. At variance with the Mn antisite defect, the total charge difference is $\Delta Z = +2$ electrons; the majority DOS component being almost unaffected with respect to the ideal case (see figure 2), the total charge variation is taken over by the peak in the DOS just below E_F in the minority component only ($\Delta N_- = +2$ electrons). In this case, the spin polarization at the Fermi level, defined as

$$P = \frac{N^{\uparrow}(E_F) - N^{\downarrow}(E_F)}{N^{\uparrow}(E_F) + N^{\downarrow}(E_F)} \tag{3}$$

where $N^{\uparrow}(E_F)$ and $N^{\downarrow}(E_F)$ respectively denote the up- and down-spin components of the total DOS at E_F, is as low as 6%. Moreover, since the tunnelling current in experiments is dominated by the s electrons, we also calculated the s component of the spin polarization at E_F, defined as

$$P_s = \frac{N_s^{\uparrow}(E_F) - N_s^{\downarrow}(E_F)}{N_s^{\uparrow}(E_F) + N_s^{\downarrow}(E_F)}. \tag{4}$$

Our result $P_s = 55\%$ is in very good quantitative agreement with experiment [26]; this excellent agreement may, however, be fortuitous, due to the uncertainties in experiments—as regards the materials quality—and in theory—due to numerical precision. As a bottom line, however, we suggest that, due to the possibility of these defects being formed, the decreased value of the measured spin polarizations—with respect to their bulk value—could be ascribed to this kind of defect, in addition to surface effects or other more complicated defects.

In order to further investigate the defect-induced states in the Co-antisite case, we plot the spin-resolved band structure in figure 4. The bold (red) line in the minority-spin bands highlights the defect-induced bands and clearly shows the extremely localized character of the state in proximity to the Fermi level. Moreover, figure 4(a) shows that the bands crossing E_F in the majority spin channel are quite highly dispersed, therefore suggesting a rather high Fermi velocity, which might prove useful in the spin-injection context. In the minority-spin bands, on the other hand, in addition to the defect-induced bands at E_F, the presence of a gap of about 0.5 eV is evident.

Further insights about the spatial localization of the defect-induced changes can be gained from an analysis of the magnetic moments of the Co defect and of their Co first-nearest neighbours (shown in figure 3(b)). As in the previous Mn-antisite case, most of the variation of the total magnetic moment with respect to the ideal value is due to the defect atomic site, whereas already the first-nearest neighbour shell largely recovers the magnetic moment typical of the bulk. This confirms the localized nature of the defect-induced changes.

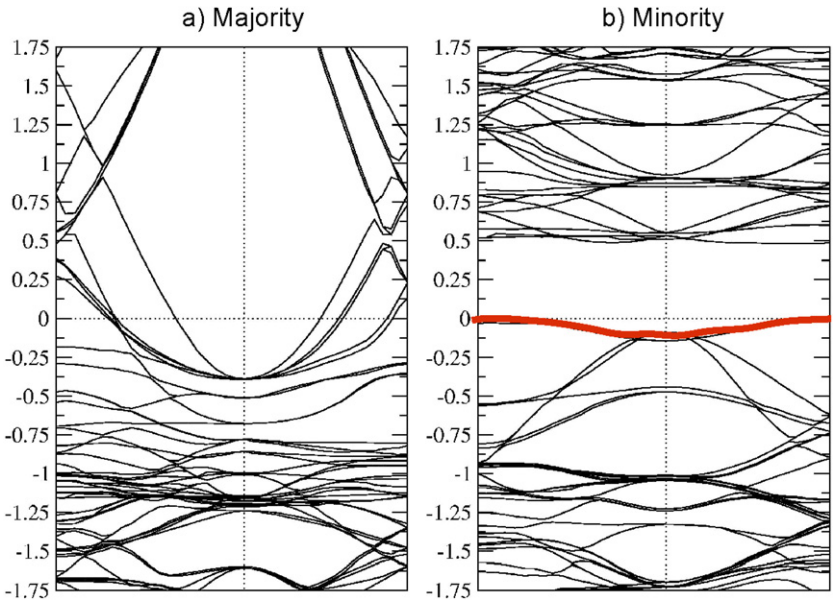

Figure 4. (a) Majority and (b) minority band structure for the Co-antisite case along the X–Γ–L symmetry line. The bold (red) line highlights the defect-induced states, located at E_F.

Let us now move to stoichiometric atomic swaps and focus on the Co–Mn swaps. The calculated integer total magnetic moment (see table 1) suggests half-metallic behaviour. Indeed, this is clearly seen in the total DOS (see figure 2(c)). A comparison with the ideal situation shows that the majority DOS is basically unaffected; on the other hand, the occupied minority DOS shows a small shift (about 0.1–0.2 eV) towards higher binding energies, along with a defect-induced peak located at -0.2 eV below E_F. Therefore, due to its energy position, this peak is not as crucial as in the Co-antisite case and half-metallicity is kept by Co–Mn swaps. Moreover, our results are in overall agreement with those reported by Orgassa *et al* [24] for NiMnSb: in the case of $Ni_{1-x}Mn_xSb$ disorder—similar to the Mn–Co swap considered here—a peak just below E_F arises in the minority spin component of the total DOS. This peak drastically broadens in energy as the concentration of defects is increased, finally reaching E_F and resulting in the loss of half-metallicity (see figure 1 of [24]). In our case, we obtain a very similar behaviour, except for the more 'energetically localized' nature of the peak; we think that this quantitative disagreement might be due to the computational method—layer Korringa–Kohn–Rostoker in conjunction with the coherent potential approximation—used in [24].

The magnetic moments (shown in figure 3(c)) in the defective region show quite an interesting behaviour: almost two Bohr magnetons are 'lost' when Co substitutes for Mn and another two Bohr magnetons are 'lost' when Mn substitutes for Co. As a result, the total magnetic moment is reduced by 4 μ_B (i.e. the difference between the bulk and defective total magnetic moments, 40 μ_B and 36 μ_B, respectively). It is also interesting to note that the swaps induce a behaviour similar to that of the single point defects, giving a sort of 'additive' effect; in fact, in this case, the magnetic moment for Mn substituting for Co is -0.83 μ_B, compared with -0.87 μ_B for the Mn antisite. Similarly, the magnetic moment for Co substituting for Mn is 1.05 μ_B, to be compared with 1.22 μ_B for the Co antisite. This shows that the first coordination

shell (similar[3] in the case of isolated point defects and for the swaps) mainly determines the behaviour of the magnetic moments, again confirming the very spatially localized character for the point defects considered.

As far as the electronic and magnetic properties of the Mn–Si swaps are concerned, a comparison between the total DOS (see figure 2(d)) in the ideal and defective cells shows only minor defect-induced changes. In particular, in the energy region around E_F, the DOS is very similar for both minority and majority spin components, resulting in the same bandgap and half-metallic character as for the pure bulk. As a result, the Mn–Si swap system shows a total magnetic moment equal to that of the ideal Heusler alloy. This is consistent with the atomic magnetic moments shown in figure 3(d): within 0.04 μ_B, the defect only results in a swap between the Mn and Si magnetic moments. Again, this shows that the first coordination shell—which in this case is exactly the same as the one in the bulk for both the exchanged atoms—is the most relevant in the formation of the bonds, local charge and spin density rearrangement and resulting magnetic moments.

3.2.1. Role of the Z (Z = Si, Ge) anion in the electronic structure of Co_2MnZ. Our calculations show that both the spatial and energy behaviour of defect-induced gap states suggests that Co antisites show a similar behaviour in Co_2MnGe and Co_2MnSi. We remark that in the Co-antisite case the loss of half-metallicity in Co_2MnGe is also shown by the non-integer total magnetic moment (see table 1), whereas for the Si-based compounds the total moment is still close to an integer value and the loss of half-metallicity is evidenced by an analysis of the total DOS. Moreover, we also calculated the defect concentrations for Co_2MnGe considering two different growth temperatures: $T_1 = 825$ K, as reported in [25] for films via pulsed laser deposition, and $T_2 = 165$ K, as reported for films grown via molecular beam epitaxy (MBE). As expected, the two different temperatures result in very different concentrations: in the case of the MBE growth, all the defects have an almost negligible probability of being formed, whereas in the higher temperature growth the concentration of Mn atoms occupying the Co site is of the order of $<1\%$ and other defects have much smaller densities.

In order to compare the behaviour of the defects considered in Co_2MnSi and Co_2MnGe, we report in parentheses in figure 3 the value of the atomic magnetic moments in the region around the defect site. The two different hosts globally show a very similar behaviour in terms of magnetic moments, suggesting that the larger lattice constant or the smaller minority bandgap of the Ge-based compound are not really relevant in the final determination of the magnetic properties. Quantitatively, the largest differences are shown by the Co-antisite case: there is about a 0.4 μ_B difference between the total magnetic moments in Co_2MnSi and Co_2MnGe (see table 1). Figure 3(b) shows that this difference is almost entirely due to differences in the central Co antisite, which changes from about -0.9 μ_B in Co_2MnSi to about -1.4 μ_B in Co_2MnGe, due to a very small difference in the energy position (<0.05 eV) of the defect-induced peak with respect to E_F.

Finally, it is interesting to note that the position of the defect-induced peak in the DOS with respect to E_F and the related energy position of the conduction band minimum in the minority spin component are very similar: for both Co_2MnSi and Co_2MnGe, the peak is basically coincident with E_F in the case of the Co antisite, whereas it lies at about -0.2 eV in the case of the Co–Mn swap. Except for very small differences that can be traced back to differences in the ideal bulk hosts (see [5] for details), the calculated DOSs for antisite and swap defects in Co_2MnGe are not shown, due to behaviour very similar to Co_2MnSi.

[3] As also shown in figure 1 in the Heusler side, when Co substitutes for Mn, it is surrounded by an octahedral cage of Co. When Mn substitutes for Co, on the other hand, it has four Mn and four Si as nearest neighbours. In the Co–Mn swap, the Mn substituting Co has seven Co and one Mn, whereas the Co substituting for Mn has three Mn, one Co and four Si atoms as nearest neighbours.

3.3. Overview of recent first-principles calculation on point defects in Heusler alloys

In this section, we report the main results of some relevant works recently published on point defects, either in half-Heusler alloys (not treated here) or focusing on other aspects of defects in Co_2MnSi and Co_2MnGe, with respect to those so far presented in this review.

We start with one of the most studied Heusler alloys: NiMnSb. Attema *et al* [27] focused on the influence of intrinsic defects as well as of finite-temperature effects in half-metallic NiMnSb. Of the 14 cases of intrinsic defects considered, five were found to affect the half-metallicity; however, these were energetically very unfavourable. Moreover, non-intrinsic defects, such as artificially doping by rare-earth or Sc atoms, as well as the effect of nano-structured contacts, were suggested to influence the magnon spectrum, therefore modifying the behaviour at finite temperature. More recently, Alling *et al* [28] performed a careful study of point defects, including nonstoichiometric antisites, interstitial and vacancy defects, as well as stoichiometric atomic swap defects. The formation energies of the defects were found to span a large range from 0.2 to 14.4 eV; moreover, the defects with low formation energies preserved the half-metallic character of NiMnSb. Some of the defects were found to increase the magnetic moment and this could explain the experimentally observed increase of magnetic moments in some samples of NiMnSb. In particular, Mn interstitials were found to increase the magnetic moment, to have a low formation energy, and to keep the half-metallic character of the material.

Miura *et al* [29] investigated the atomic disorder effects on the half-metallicity of the full-Heusler alloy $Co_2(Cr_{1-x}Fe_x)Al$ from first principles by using the Korringa–Kohn–Rostoker method with the coherent potential approximation. The disorder between Cr and Al was not found to significantly reduce the spin polarization of the parent alloy Co_2CrAl, while disorder between Co and Cr lead to a considerable reduction of the spin polarization. The spin polarization of $Co_2(Cr_{1-x}Fe_x)Al$ was observed to decrease with increasing Fe concentration x in both the ordered $L2_1$ and the disordered $B2$ structures, and the effects of the disorder on the spin polarization is significant at low Fe concentrations. The authors suggested that a highly spin-polarized ferromagnet with high Curie temperature might be obtained if a $Co_2(Cr_{1-x}Fe_x)Al$ with the ordered $L2_1$ structure could be fabricated at low Fe concentrations.

An accurate density-functional study, focused on the effect of crystalline imperfections on the band-structure of Co_2MnGe, was performed by Carey *et al* [30]. In particular, the authors examined the effects on the half-metallicity of (i) uniform and tetragonal distortions and (ii) extrinsic dopants such as Cu, Al, O, Rh, and Sn impurities. A high spin polarization could be maintained even under significant strains and distortions. However, the authors found even an extrinsic-impurity concentration as low as 3% to generally have a dramatic effect on the half-metallic behaviour of the Heusler alloy. More recently, Galanakis *et al* [31] investigated the effect of doping and disorder on the Co_2MnGe electronic and magnetic properties. They found that doping by substituting Fe or Cr for Mn marginally affected the half-metallicity. A similar effect was also achieved by mixing the sublattices occupied by the Mn and sp atoms. Therefore, the authors concluded half-metallicity to be a robust property of these alloys.

Furthermore, the electronic structures were systematically calculated by Ishida *et al* [32] for many Heusler alloys X_2YZ (X and Y = 3d transition element, Z = IIIb, IVb, Vb element); it was found that Fe_2CrZ alloys show a high density of states at the Fermi energy in the majority-spin state, as well as a large spin polarization. The effects of several types of chemical disorder on the half-metallicity and magnetic moment were discussed in terms of the related electronic structures. Among the Fe_2CrZ alloys the authors found several highly spin polarized materials to be insensitive to chemical disorder and they pointed out that Fe–Cr chemical disorder is likely to occur.

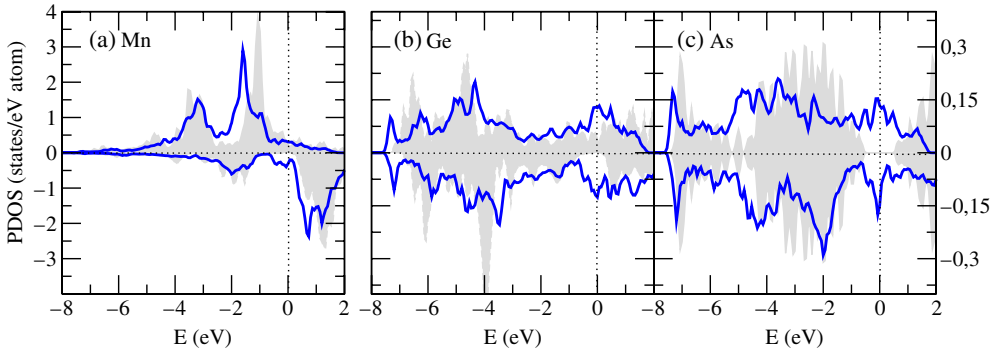

Figure 5. PDOS for (a) Mn, (b) Ge and (c) As in the Co_2MnGe/GaAs junction (Mn–Ge and As termination), shown by the thick (blue) solid lines. The dashed grey areas show the corresponding PDOS in bulk Co_2MnGe and GaAs.

4. Interfaces with semiconductors: results and discussion

4.1. Loss of half-metallicity at the interface

In figure 5 we show the partial density of states (PDOS) for the atoms close to the junctions in the Co_2MnGe/GaAs case (Mn–Ge and As termination). For comparison, we also show the corresponding PDOS in ideal bulk Co_2MnGe and GaAs. The most remarkable feature is that the half-metallic and semiconducting character, shown respectively by the Heusler and the SC in their bulk phase (see shaded areas in figure 5), is completely lost at the interface: interface states fully occupy the gap. A careful analysis of the origin of these states shows that they result from the strong hybridization of Mn d and As p states, and, to a lesser extent, from Ge p orbitals. The situation is therefore dramatically different from the case of defect states: as previously observed, defect-induced states are very narrow in energy and the 'perturbation' is essentially localized around the defective atom; on the other hand, interface states are very broad in energy and the 'perturbation' is, due to strong hybridization effects, much stronger and spatially more extended. Furthermore, we remark that the loss of half-metallicity at the interface was similarly observed in all the junctions considered, irrespective of the junction atomic termination (Co versus Mn–Ge, As or Ga) or of the SC materials (GaAs versus Ge). As a general remark, we therefore note that careful features in the DOS at the interface must be taken into account when designing Heusler/SC interfaces for spin-injection purposes, since the predicted 100% spin polarization can be degraded in proximity to the junction.

As for the spatial character of the interface states [33], the analysis of the PDOS for atoms as we move away from the interface (not reported), both on the Co_2MnGe and on the SC side, shows that interface states are rather well screened in both parts. In particular, a few layers away from the junctions are sufficient to fully recover half-metallicity in Co_2MnGe; on the GaAs side, interface states are very efficiently screened and the recovery is even faster. Incidentally, this shows that the size of our supercell is sufficiently large to guarantee a realistic simulation of the junction made up of ideally semi-infinite parts.

4.2. Degree of spin polarization

Since spin-injection from a Heusler into semiconductors is such a relevant point, we give here some further information on transport properties, in terms of the degree of spin polarization (DSP) as well as of Fermi velocities. Recall that Mazin [34] proposed different definitions of

Table 2. Density of states at E_F for the majority ($N_\uparrow(E_F)$) and minority ($N_\downarrow(E_F)$) spin channels, along with the corresponding Fermi velocities ($v_{\uparrow F}$ and $v_{\downarrow F}$ for the up and down spins, respectively) resolved in the parallel and perpendicular components, with respect to the [001] ordering direction. Density of states and Fermi velocities are reported in states/(eV cell) and 10^7 cm s^{-1}, respectively.

	$N_\uparrow(E_F)$	$N_\downarrow(E_F)$	$v^{\parallel}_{\uparrow F}$	$v^{\perp}_{\uparrow F}$	$v^{\parallel}_{\downarrow F}$	$v^{\perp}_{\downarrow F}$
$Co_2MnGe/GaAs$	10.7	10.4	1.44	0.38	0.56	0.12
Co_2MnGe/Ge	8.9	5.6	2.46	0.51	1.41	0.12

Table 3. Degree of spin polarization, using the different proposed definitions, for $Co_2MnGe/GaAs$ and Co_2MnGe/Ge junctions.

	P_0 (%)	$P_1^{\parallel}$ (%)	$P_1^{\perp}$ (%)	$P_2^{\parallel}$ (%)	$P_2^{\perp}$ (%)
$Co_2MnGe/GaAs$	1	44	53	74	82
Co_2MnGe/Ge	23	47	75	66	94

DSP, each to be used in a specific regime. In particular, the most natural and popular definition involves the DOS at the Fermi level for the majority and minority spin channels and is probed in spin-polarized photoemission measurements:

$$P_0 = [N_\uparrow(E_F) - N_\downarrow(E_F)]/[N_\uparrow(E_F) + N_\downarrow(E_F)]. \tag{5}$$

However, in transport measurements, Fermi velocities are of course relevant quantities and should therefore be involved in the spin-polarization definition. In particular, for low-resistance ballistic contacts, the appropriate definition is

$$P_1 = [\langle N(E_F)v_F\rangle_\uparrow - \langle N(E_F)v_F\rangle_\downarrow]/[\langle N(E_F)v_F\rangle_\uparrow + \langle N(E_F)v_F\rangle_\downarrow] \tag{6}$$

whereas for large barrier and/or diffusive currents the correct definition is

$$P_2 = [\langle N(E_F)v_F^2\rangle_\uparrow - \langle N(E_F)v_F^2\rangle_\downarrow]/[\langle N(E_F)v_F^2\rangle_\uparrow + \langle N(E_F)v_F^2\rangle_\downarrow] \tag{7}$$

where $\langle\ \rangle$ denotes the Fermi surface average.

In table 2, we report the spin-resolved values of the density of states at the Fermi level ($N(E_F)$) and the Fermi velocities (v_F) in the $Co_2MnGe/GaAs$ and Co_2MnGe/Ge interfaces. As far as Fermi velocities are concerned, we remark that, due to the anisotropic geometry, there are two different velocities, parallel and perpendicular to the [001] growth axis. Moreover, using these calculated values in the previous different definitions of P, we obtain the degree of spin polarization for the different interfaces, as reported in table 3.

We note the following. (i) In the case of $Co_2MnGe/GaAs$ the up and down spin DOSs at E_F have more or less the same value, whereas there is a larger imbalance in the Co_2MnGe/Ge case; consistently, when these values are used in the evaluation of P_0, there is a negligible polarization in the GaAs case and a slightly larger one in the Ge case. None of them, however, seems promising for spin-injection purposes. (ii) The Fermi velocities look highly anisotropic, with the parallel velocities larger than the perpendicular geometry, due to the large (small) dispersion of the bands in plane (out of plane): this is consistent with our choice of an anisotropic tetragonal unit cell, which shows a large c/a ratio. Moreover, for both systems, the majority Fermi velocities are much higher than those in the minority spin channel, consistent with that previously observed when discussing figure 4 and, more generally, with the character of the bands crossing E_F in the Co_2MnGe compound [6, 5]. (iii) As a consequence of the previous point, P_1 and P_2 have in general much larger values than P_0. In particular, very high values of DSP (of the order of 90%) are reached in the diffusive regime in the perpendicular

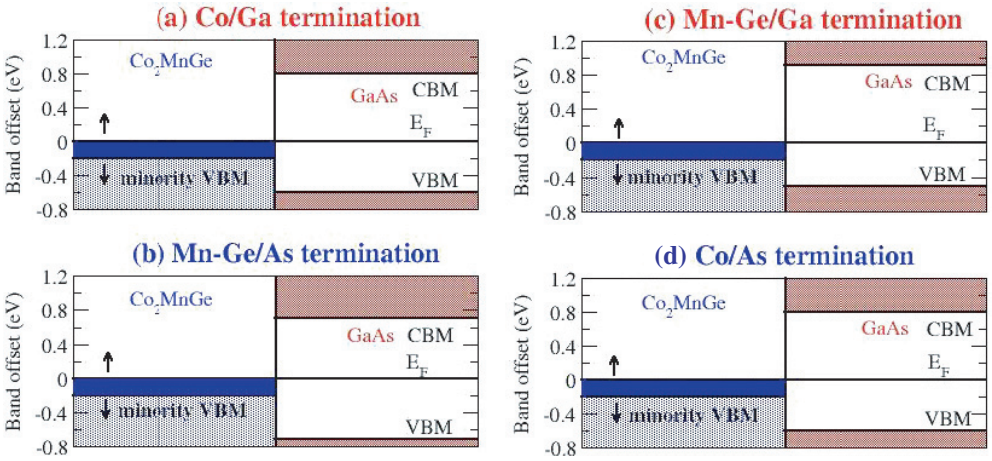

Figure 6. Potential line-up for the Co_2MnGe/GaAs interface with different terminations: (a) Co/Ga terminated, (b) Mn–Ge/As, (c) Mn–Ge/Ga and (d) Co/As. The Fermi level is set to zero of the ordinate scale. On the left side, the hatched (blue) area on the Heusler side shows the minority spins, whereas the dark (blue) region shows the majority spins; on the right side, the hatched (red) area shows the valence and conduction bands.

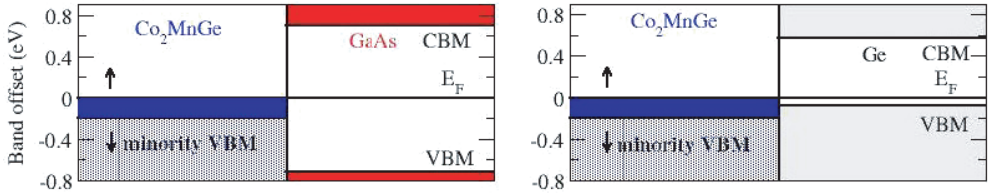

Figure 7. Potential line-up for the Co_2MnGe interfaced with GaAs (left panel) and Ge (right panel). The termination is Mn–Ge on the Heusler side and As in the GaAs side. The Fermi level is set to zero of the ordinate scale.

direction; relatively high values are also obtained in the ballistic regime along the perpendicular axis, which makes the proposed junction quite appealing in the spintronics framework.

4.3. Spin resolved band line-up

We now focus on the band line-up at the Co_2MnGe/SC junction, evaluated in all-electron calculations similar to what is done in photoemission experiments, i.e. by taking core levels as reference energies and considering both *bulk* and *interface* contributions [35]. Our results for the Co_2MnGe/GaAs junctions are presented in figure 6, where we show (i) the position of E_F with respect to the SC VBM, giving rise to a p-type SBH for the majority spin carriers, $\Phi^{\uparrow}_{B_p}$, and (ii) the position of the VBM for the minority-spin states with respect to the SC VBM, giving rise to a valence band offset for the minority spin carriers, $VBO^{\downarrow}$. The position of E_F with respect to the SC conduction band minimum (CBM), denoted as $\Phi^{\uparrow}_{B_n}$, has been obtained considering the experimental energy gap (due to the strong underestimation of the bandgap within DFT) for GaAs and Ge ($E_{gap} = 1.5$ eV and $E_{gap} = 0.7$ eV, respectively) [36] so that $\Phi^{\uparrow}_{B_n} = E_{gap} - \Phi^{\uparrow}_{B_p}$.

In figure 6, we show the potential line-up of Co_2MnGe/GaAs junctions as a function of different terminations; on the other hand, in figure 7, we show the band-offset when changing

the SC, i.e. GaAs and Ge. Our results show that (i) the charge rearrangement at the interface is largely dependent on the SC material and (ii) in both SCs the E_F level is *pinned* at an energy position similar to that obtained with other non-magnetic metals (e.g. the SBH is 0.07 (0.18) eV for Ge/Au (Ge/Al), 0.52 (0.62) eV for GaAs/Au (GaAs/Al)) [37]. This suggests that spin-polarization effects do not play an important role in the potential line-up, which is therefore predictable on the basis of non-spin-polarized SBH. On the other hand, *ab initio* calculations are essential to predict spin-polarized-metal/SC junctions where interface gap states do not reduce the spin polarization at the junction [38]. Furthermore, consistent with the pinning mechanism previously outlined for GaAs, different atomic terminations in Co_2MnGe/GaAs result in changes of at most 0.2 eV in the potential line-up, though not affecting the rectifying character of the case shown. Therefore, as far as possible applications in spintronics are concerned, in the case of Heusler/GaAs junctions, the presence of a Schottky barrier may be useful for spin-injection purposes: the rectifying region was one of the mechanisms proposed to reduce the conductivity mismatch [39] between the spin-polarized source and the semiconductor, which is believed to strongly reduce the efficiency for injection of highly polarized currents. The contact character shown in figure 7 for the Ge case may also be useful for spin-injection purposes, Co_2MnGe being in this case a source of spin-polarized holes to be injected into the Ge side. However, we need to point out that electrons have longer lifetimes and higher mobilities than do holes, hence, so far, greater interest has been devoted to materials that could inject spin-polarized electrons rather than holes.

4.4. Overview on recent first-principles calculation on interfaces between Heusler alloys and semiconductors

Similar to what we have done in the case of point defects, we report here an overview on density-functional simulations performed for full- or half-Heusler alloys when interfaced with a semiconductor and which focused on different issues or materials than those presented so far.

Pioneering calculations were performed by de Groot and co-workers [38] for NiMnSb interfaces. They showed that half-metallicity is generally lost at interfaces with semiconductors, except in the case of [111]-ordered interfaces with CdS. Therefore, the authors concluded that a proper engineering of the junction region at the atomic level might lead towards a 100% spin-polarized charge injection.

More recently, Galanakis *et al* [40] studied the electronic and magnetic properties of the interfaces between the half-metallic Heusler alloy NiMnSb and the binary semiconductors InP and GaAs. Although in the case of most NiMnSb/InP(001) contacts the half-metallicity was lost, the authors suggested that a high degree of spin polarization could be obtained when the interface consisted of Ni and P layers. In the case of GaAs, the larger hybridization between the Ni d and As p orbitals with respect to the hybridization between the Ni d and P p orbitals was found to destroy this polarization. The (111) interfaces showed strong interface states, but also in this case the authors identified a few interfaces presenting a high spin polarization at the Fermi level (as high as 74%). Along a similar line, another paper [41] focused on Co_2CrAl/InP junctions, Galanakis identified mechanisms that could keep high spin polarization at the interface (more than 80% of the electrons at the Fermi level of majority spin) although the full half-metallicity is lost. For example, the large enhancement of the Cr moment at the interface between a CrAl-terminated Co_2CrAl(001) spacer and the InP(001) semiconductor was found to weaken the effect of the interface states, thus resulting in a high spin polarization. On the other hand, the Co_2CrAl/InP interfaces terminated by a Co layer and either In or P showed a severe decrease of the Co spin moment, but Cr in the subinterface layer was found to be bulk-like, so that the resulting spin polarization was calculated to be similar to that of the CrAl-terminated interfaces.

The NiMnSb/GaAs(001) heterojunction was also investigated by Debernardi *et al* [42] by means of pseudopotential local spin density calculations. The half-metallicity was found to be generally lost when joining NiMnSb with the semiconductor, even at the interface with a mixed (Mn, As) plane which is one of the most promising for maintaining the desired half-metallicity. In this case, however, the effect was localized just on the interfacial atoms. Electronic and magnetic bulk properties were recovered within a couple of atomic planes far from the interface, so that the band alignments were well defined.

Very recently, the electronic properties of Co_2CrAl/GaAs interfaces were investigated by using first-principles calculations within density functional theory [43]. The spin polarization was calculated to remain relatively high at the (110) interface and to reach almost unity for a specific (110) interfacial structure. Furthermore, the nearly half-metallic interface turned out to be the most stable of the (110) interfacial structures studied. In order to eliminate the effects stemming from the localized d component, the spin polarization calculated only from the sp-projected density of states was also examined and showed that the high spin polarization at the (110) interface owes little to the localized d component and, therefore, is expected to be fairly relevant to transport properties. Co_2CrSi/GaAs, Co_2MnSi/GaAs, and Co_2MnGe/GaAs heterostructures were also investigated, resulting in a similar half-metal-like behaviour at the (110) interface.

5. Conclusions

We have presented a review of first-principles simulations performed for the Co_2MnGe and Co_2MnSi Heusler alloys, mainly focusing on their junctions with standard semiconductors and intrinsic defects. Several mechanisms for the loss of half-metallicity, the Heusler peculiar characteristic so desirable for spintronic applications, have been proposed. In particular, point defects—such as antisites and atomic swaps—have been studied: Mn antisites were found to keep half-metallicity, whereas Co antisites were suggested to be detrimental, due to the presence of defect-induced states at the Fermi level. For both nonstoichiometric defects, the formation energy was calculated to be pretty low, in excellent consistency with the experimental observation of a high degree of disorder in the Co and Mn sublattices. As far as Heusler/semiconductors are concerned, we found that the strong hybridization between transition-metal d bands and sp hybrids in the semiconducting side gives rise to gap states, destroying half-metallicity. The band line-up was found to depend negligibly on the interface atomic termination, whereas it was strongly affected by the specific semiconductor: for GaAs the contact was predicted to be strongly rectifying, whereas in the Ge case the Fermi level lies close to the valence band maximum, more similar to an Ohmic contact.

In summary, we remark that despite the strong experimental and theoretical interests recently devoted to Heusler alloys, this class of materials is not sufficiently understood so far. On the experimental side, the materials' quality is still rather poor and stronger efforts should be devoted to improve it, by a careful engineering of the crucial growth parameters. On the theoretical side, a lot of work has been performed for half-metals, but a lot remains to be done. For example, almost unexplored though promising territories include (i) the simulation of magnetic tunnel junctions focused on predicting tunnelling-magnetoresistance ratios or (ii) magnetically doped half-Heusler compounds (such as Mn- and Cr-doped NiTiSn or CoTiSb) [44, 45]. Despite the crowded class of predicted half-metals (including diluted magnetic semiconductors, Sr-doped manganites, etc), the high Curie temperatures and the crystallographic compatibility with common semiconductors of Heusler compounds still represent two appealing qualities in the spintronics framework, so that a technological breakthrough coming from these materials in the next few years seems not to be unlikely.

References

[1] Kämmerer S, Thomas A, Hütten A and Reiss G 2004 *Appl. Phys. Lett.* **85** 79
[2] Sakuraba Y, Nakata J, Oogane M, Kubota H, Ando Y, Sakuma A and Miyazaki T 2005 *Japan. J. Appl. Phys.* **35** L1100
[3] Dong X Y, Adelmann C, Xie J Q, Palmstrom C J, Lou X, Strand J, Crowell P A, Barnes J-P and Petford-Long A K 2005 *Appl. Phys. Lett.* **86** 102107
[4] Fujii S, Sugimura S, Ishida S and Asano S 1990 *J. Phys.: Condens. Matter* **2** 8583
Ishida S, Fujii S, Kashiwagi S and Asano S 1995 *J. Phys. Soc. Japan* **64** 2152
[5] Picozzi S, Continenza A and Freeman A J 2002 *Phys. Rev.* B **66** 094421
[6] Galanakis I and Dederichs P H (ed) 2006 *Half-metallic Alloys: Fundamentals and Applications* (*Lecture Notes in Physics*) (Berlin: Springer)
[7] Lezaic M, Mavropoulos Ph, Enkovaara J, Bihlmayer G and Blügel S 2006 *Phys. Rev. Lett.* **97** 026404
[8] Kandpal H C, Fecher Gerhard H, Felser C and Schönhense G 2006 *Phys. Rev.* B **73** 094422
[9] Ishida S, Masaki T, Fujii S and Asano S 1998 *Physica* B **245** 1
[10] Hashemifar S J, Kratzer P and Scheffler M 2006 *Phys. Rev. Lett.* **94** 096402
[11] Galanakis I 2002 *J. Phys.: Condens. Matter* **14** 6329
[12] Kübler J, Williams A R and Sommers C B 1983 *Phys. Rev.* B **28** 1745
[13] Kawakami M, Kasamatsu Y and Ido H 1987 *J. Magn. Magn. Mater.* **70** 265
[14] Von Barth U and Hedin L 1972 *J. Phys. C: Solid State Phys.* **5** 1629
[15] Perdew J P, Burke K and Erzenhof M 1996 *Phys. Rev. Lett.* **77** 3865
[16] Wimmer E, Krakauer H, Weinert M and Freeman A J 1981 *Phys. Rev.* B **24** 864
[17] Monkhorst H J and Pack D J 1976 *Phys. Rev.* B **13** 5188
[18] Koelling D D and Wood J H 1986 *J. Comput. Phys.* **67** 253
[19] Picozzi S, Continenza A and Freeman A J 2004 *Phys. Rev.* B **69** 094423
[20] Zhang S B *et al* 1993 *Phys. Rev.* B **57** 9642
[21] Asada T and Terakura K 1993 *Phys. Rev.* B **47** 15992
[22] Van de Walle C G *et al* 1993 *Phys. Rev.* B **47** 9425
[23] Raphael M P, Ravel B, Huang Q, Willard M A, Cheng S F, Das B N, Stround R, Bussmann K M, Claassen J H and Harris V G 2002 *Phys. Rev.* B **66** 104429
[24] Orgassa D, Fujiwara H, Schulthess T C and Butler W H 1999 *Phys. Rev.* B **60** 13237
[25] Ambrose T, Krebs J J and Prinz G A 2000 *J. Appl. Phys.* **87** 5463
[26] Raphael M, Ravel B, Willard M, Cheng S, Das B, Stroud R, Bussmann K, Claassen J and Harris V 2001 *Appl. Phys. Lett.* **79** 4396
[27] Attema J J, Fang C M, Chioncel L, de Wijs G A, Lichtenstein A I and de Groot R A 2004 *J. Phys.: Condens. Matter* **16** S5517
[28] Alling B, Shallcross S and Abrikosov I A 2006 *Phys. Rev.* B **73** 064418
[29] Miura Y, Nagao K and Shirai M 2004 *Phys. Rev.* B **69** 144413
[30] Carey M J, Block T and Gurney B A 2004 *Appl. Phys. Lett.* **85** 4442
[31] Galanakis I, Ozdogan K, Aktas B and Sasioglu E 2006 *Appl. Phys. Lett.* **89** 042502
[32] Ishida S, Mizutani S, Fujii S and Asano S 2006 *Mater. Trans.* **47** 464
[33] Picozzi S, Continenza A and Freeman A J 2003 *J. Appl. Phys.* **94** 4723
[34] Mazin II 1999 *Phys. Rev. Lett.* **83** 1427
[35] Massidda S, Min B I and Freeman A J 1987 *Phys. Rev.* B **35** 9871
[36] *Landolt-Börnstein-Group III Condensed Matter* 1995 (Berlin: Springer) p 287
[37] Tersoff J 1986 *J. Vac. Sci. Technol.* B **4** 1066
[38] de Wijs G A and de Groot R A 2001 *Phys. Rev.* B **64** 020402
[39] Schmidt G, Ferrand D, Molenkamp L W, Filip A T and van Wees B J 2000 *Phys. Rev.* B **62** R4790
[40] Galanakis I, Lezaic M, Bihlmayer G and Blügel S 2005 *Phys. Rev.* B **71** 214431
[41] Galanakis I 2004 *J. Phys.: Condens. Matter* **16** 8007
[42] Debernardi A, Peressi M and Baldereschi A 2005 *Comput. Mater. Sci.* **33** 263
[43] Nagao K, Miura Y and Shirai M 2006 *Phys. Rev.* B **73** 104447
[44] Nanda B R K and Dasgupta I 2005 *J. Phys.: Condens. Matter* **17** 5037
[45] Sanyal B 2006 private communication